Progress In Electromagnetics Research C, Vol. 62, 11–22, 2016

Printed Compact Lens Antenna for UHF Band Applications

Koyadan Koroth Ajith* **and Amitabha Bhattacharya**

Abstract—A new microwave lens antenna suitable for ultra-high frequency (UHF: 300 MHz–3 GHz) band applications is proposed. An improved bow-tie antenna and a planar metamaterial lens design is presented. 5 dB improvement in boresight gain and a directive radiation pattern is achieved with the lens. The application of the designed antenna is demonstrated in a ground penetrating radar (GPR) experiment. The size of the antenna is very compact compared to other antennas found in the literature used for similar applications.

1. INTRODUCTION

The crucial requirements for a GPR antenna are: ultrawide bandwidth at low frequency of operation and high front-to-back ratio, keeping moderately good gain and radiation efficiency to meet the power budget. Resistively loaded bow-tie antenna is suitable for GPR applications because of its ultra-wide bandwidth and its ability to radiate short pulses. However, radiation efficiency has been very low for typical resistively loaded antennas due to lot of power dissipated in the resistors. Wu et al. [1] proposed a cavity backed, half ellipse shaped antenna with lumped resistor loading to suppress any reflections from the end. Wang et al. described the design of bow-tie antennas with high radiation efficiency [2]. Lestari et al. [3] proposed bow-tie antenna with lumped resistors loading. In their paper, time domain pulse radiating ability of the antenna was analyzed. Frequency domain antenna parameters of this antenna, such as the radiation pattern, gain and front-to-back ratio, were not discussed by them. In [4] capacitive slots were cut on the arms of the bow-tie, and microwave absorbers were put on each arm, to provide a combined resistive and capacitive loading. Absorbers on the back side of the antenna also helped in suppressing back-lobe. The impedance bandwidth (VSWR 2:1) of this antenna was from 0.5 to 5.1 GHz. A stable radiation pattern was obtained up to about 3 GHz. The input impedance was 100 Ω making it difficult to feed directly using a coaxial cable. Uduwawala et al. [5] gave a detailed study of bow-tie antenna with resistor loaded at the ends. Vee dipole antennas [6, 7] were also considered for GPR applications. Logarithmic spiral antenna [8] is another candidate for similar applications at UHF bandwidth.

The advent of microwave lens antennas dates back to 1946 when Kock [9] introduced metal lens antennas by producing artificial dielectrics. Artificial lenses are preferred over dielectric lenses at microwave frequencies because the latter tends to be bulky and heavy. A planar lens is in many ways advantageous compared to a convex lens. Planar lens is easy to fabricate and is less bulky. Pozar proposed a planar lens in [10]. Microwave lenses have evolved using concepts of geometrical optics. Most of the lens designs in literature are concerned with GHz frequencies. Lens antennas have a great potential that bandwidth independent antennas can be made if we can design the lens with desirable properties. Waveguides are the simplest examples of artificial dielectrics having refractive index less than unity since inside the waveguide, phase velocity is greater than the velocity in free space. Studies on single-layer

Received 27 November 2015, Accepted 31 January 2016, Scheduled 4 February 2016
* Corresponding author: Koyadan Koroth Ajith (ajithkkoroth@gmail.com).
The authors are with the Department of Electronics & Electrical Communication Engineering, Indian Institute of Technology Kharagpur, India.

planar lenses have been found scarce in the literature. Lens designs at sub-GHz frequencies are even more scarce. With the increasing popularity of metamaterials, the planar lens antennas are becoming popular again. Manipulation of electromagnetic fields by metamaterial is extensively discussed in [11].

Zhu et al. [12] presented a metamaterial superstrate for conversion from linear to circular polarization. They also obtained an improvement in antenna gain. Improvement of directivity of Vivaldi antenna has been presented in [13]. Qi et al. [14] succeeded in controlling the radiation pattern over a bandwidth from 12 to 18 GHz. This is a significant effort because metamaterials are inherently narrowband structures. Planar folded dipole antennas [15] were also used with metamaterials. Erentok et al. [16, 17] have done work with sub-GHz frequency metamaterials.

In this paper, we describe a resistively loaded bow-tie antenna and its improvement in performance characteristics with the application of a planar lens. Some of the results have been presented in a conference paper [18]. The experimental results including GPR scan result for detecting an object buried under soil are described in this paper. The rest of the paper is organized in three sections. In Section 2, the design of the antenna is presented in detail. Section 3 describes measurement results and discussions on it while Section 4 concludes the work.

2. ANTENNA DESIGN

2.1. Improved Bow-Tie Antenna Design

Bow-tie antennas have been studied systematically by a number of researchers by using conformal transformation. DuHamel and Isbell [19] described the design of frequency independent antennas including bow-tie antenna and showed that it can be transformed to a pair of coplanar lines by a simple conformal mapping. Carrel [20] derived expressions for the characteristic impedance of infinite coplanar fin antenna. Most of the bow-tie antenna designs have been optimized for $100\,\Omega$ input impedance. Recent developments on the analysis of printed coplanar strips based on conformal mapping [21, 22] have added to our understanding of bow-tie antenna. Ideally, a bow-tie antenna is infinite in extent and is specified only by angles. But in practice, the antenna has to be finite and can be considered as a broadband antenna with a stable radiation characteristics over the bandwidth. A bow-tie antenna with a flare angle θ and radius r is represented in the polar coordinates by,

$$z = re^{j\theta} \tag{1}$$

This analytic function can be conformally transformed into w-plane by the function,

$$w = \ln r + j\theta \tag{2}$$

Figure 1(a) shows the pictorial representation of the bow-tie antenna in the z-plane described by Eq. (1), and its conformal transformation in the w-plane, represented by Eq. (2) in Fig. 1(b). Fig. 1(c) represents the elliptical bow tie. Consider the elliptical arm as composed of narrow strips of concentric circles. Each circular strip transforms to a rectangular strip in the w plane. By joining all these strips together we get the conformal transformation in Fig. 1(d), a gradually tapered coplanar transmission line. The

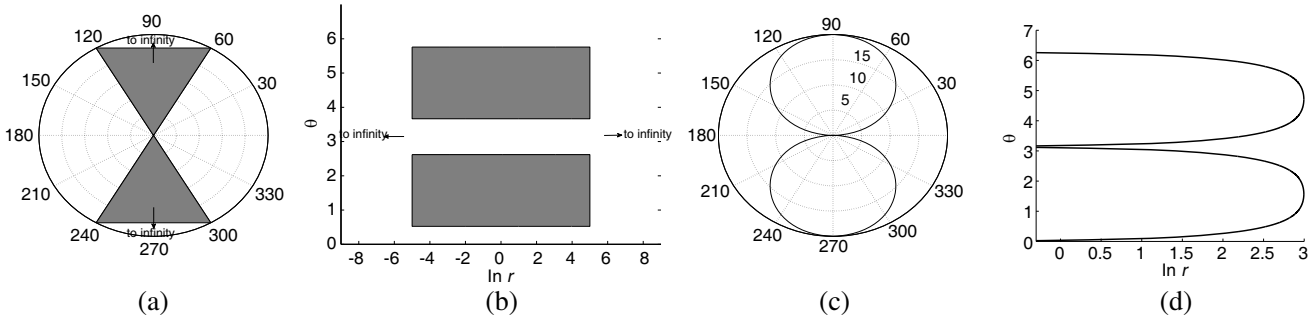

Figure 1. Conformal transformation. (a) Infinite bow-tie. (b) Conformal transformation of (a). (c) Elliptical bow-tie. (d) Conformal transformation of (c).

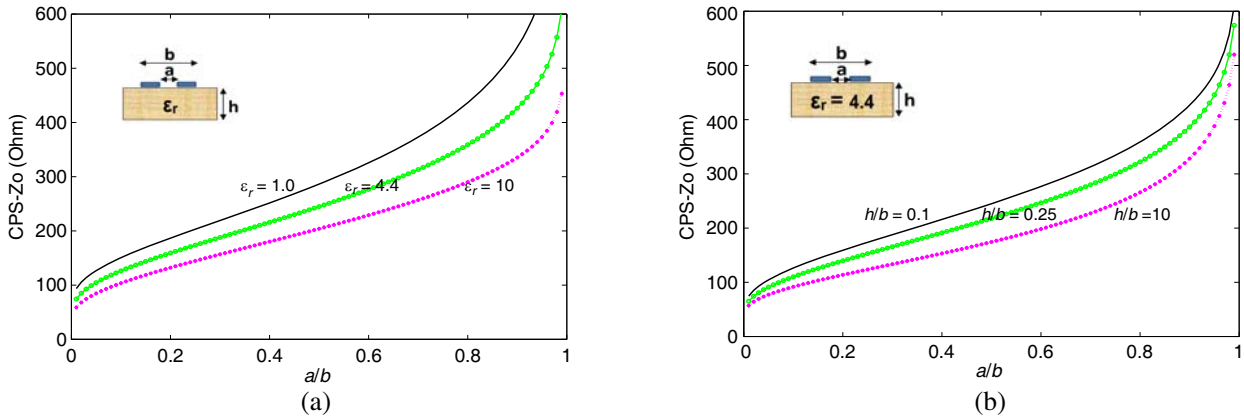

Figure 2. Characteristic impedance of coplanar stripline. (a) Characteristic impedance variation of coplanar stripline w.r.t. substrate permittivity. (b) Characteristic impedance variation of coplanar stripline w.r.t. its dimensions.

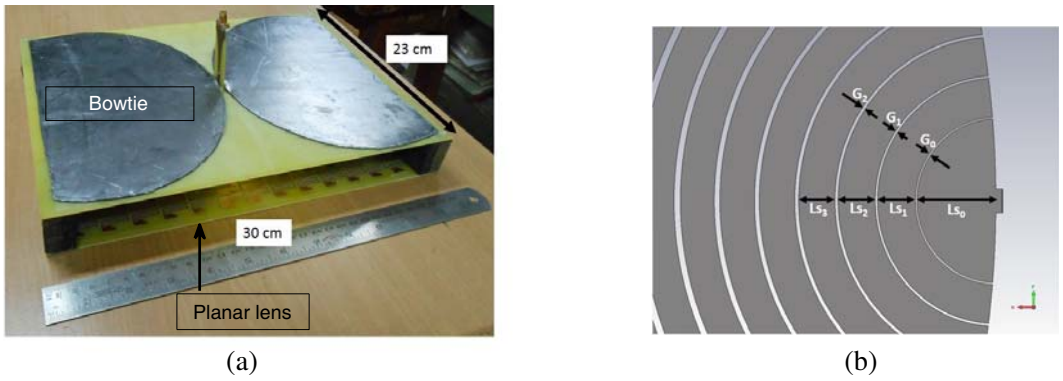

Figure 3. Final prototype of bow-tie antenna. (a) Photograph of the fabricated bow-tie antenna. (b) The arm of the bow tie.

variation of characteristic impedance of the twin strip line is shown in Fig. 2(a) as obtained from [23]. The dimensions are shown in the inset of the figure. It can be seen from the figure that, as a/b ratio decreases, the characteristic impedance also decreases. So in the case of elliptical bow-tie we initially have a lower characteristic impedance. It is also known from Carrel [20] that the impedance of the bow-tie antenna decreases as the flare angle increases. Fig. 2(b) shows variation of characteristic impedance when relative permittivity is 1, 4.4 and 10. An FR4 substrate with a relative permittivity 4.4 and thickness 1.5 mm has been chosen in this design.

The feed point impedance will depend on the curvature of the ellipses and can be optimized to give a gradual transition in the input impedance to match 50 Ω so that it can be fed easily with a microstrip to parallel strip line transition.

Concentric slots are cut on the elliptical arm in order to provide a resistive loading. The designed antenna is an RC-loaded bow tie inspired by Lestari et al. [4] with some modifications. The antenna is fed with a 50 Ω coax through a microstrip to parallel strip line transition. An artificial dielectric lens is then placed in front of the antenna to focus the radiation.

Figure 3(a) shows the fabricated bow tie with lens. Fig. 3(b) gives a close look at one arm of the bow tie at the feed location. A sheet of graphite of 1 mm thickness is put over each arm to obtain resistive loading. The resistivity of graphite has been determined by using Hall effect measurement and is 1.33×10^{-4} Ωcm. Various design parameters with reference to Fig. 3(b) are:

$Ls_0 = 10$ mm, $Ls_1 = 4.8$ mm, $Ls_2 = 4.7$ mm, $Ls_3 = 4.6$ mm ... and so on.

$G_0 = 0.2$ mm, $G_1 = 0.3$ mm, $G_2 = 0.4$ mm ..., etc.

The slot width increases as we move away from the feed point and hence the effective resistive loading increases towards the end. The overall size of the antenna is $30 \times 23\,\mathrm{cm}^2$.

2.2. Metamaterial Lens

Figure 4 depicts the focusing action using artificial materials. In the figure, medium 1 represents air, and medium 2 represents a material belonging to the particular quadrant. The quadrant 1 materials are DPS (Double Positive) materials, and quadrant 3 represents the DNG (Double Negative) materials. These two types of materials can be utilised for lens application. Quadrants 2 and 4 media do not allow the wave to propagate.

A planar lens has been designed by introducing metallic pattern inclusions on an FR4 epoxy substrate as shown in Fig. 5(a). The metallic inclusions serve to increase the refractive index of the

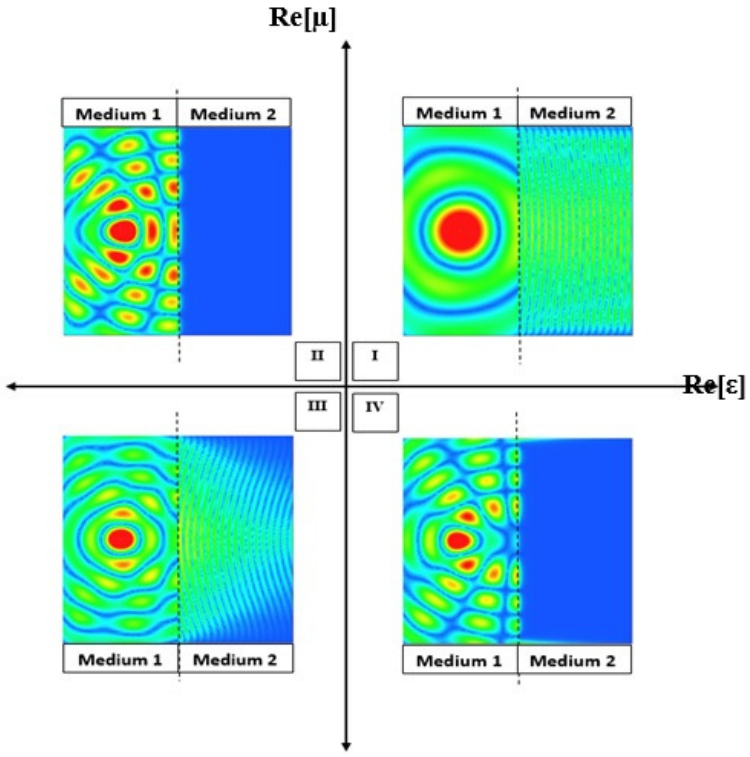

Figure 4. Focusing action by materials in first and third quadrants.

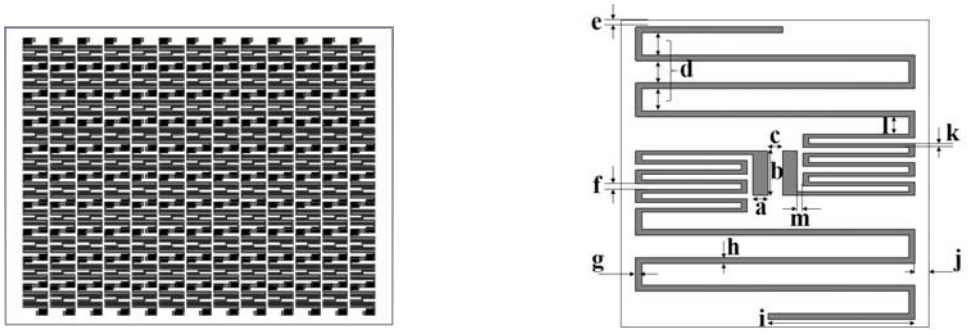

(a) (b)

Figure 5. Metamaterial lens. (a) Designed 13×10 array of unit cells. (b) The unit cell from [16].

Table 1. Design values in mm.

a	2	e	0.2774	h	1	k	0.5
b	3	f	0.2	i	10	l	1.1938
c	1	g	1	j	1	m	0.2
d	0.6096						

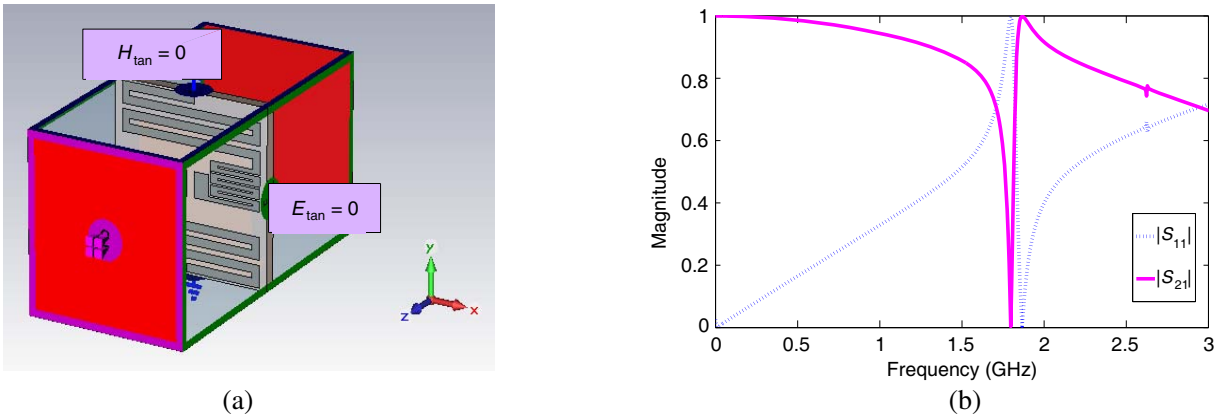

(a) (b)

Figure 6. Simulation of the unit cell in CST Microwave Studio. (a) Simulation setup. (b) Magnitude of S_{21} vs. frequency.

medium. But one has to be careful to minimize the reflections from the lens surface. The basic unit cell is from the paper by Erentok et al. [16] shown in Fig. 5(b). Erentok et al. used their design with lumped element loading, and the material was a narrow-band volumetric metamaterial. But in this work the ENG unit cell from their design is optimized for lens design. It has been used without the lumped elements and has been found to have a very broad band response. The final designed values of unit cell dimensions are given in Table 1. The simulation is carried out with the time-domain solver in CST microwave studio with the boundary conditions shown in Fig. 6(a). Perfect electric and perfect magnetic boundary conditions have been applied on the boundaries parallel to y-axis and x-axis, respectively. In z-direction, open boundary conditions have been applied. This simulates an array of unit cells, infinite in extent in x and y directions. The transmission S parameter obtained from this simulation is shown in Fig. 6(b). The size of the unit cell at 300 MHz is only $\lambda/50$. At 3 GHz, the unit cell size is $\lambda/5$. Between these frequencies, the lens acts like a resonant metamaterial and can exhibit a negative refractive index. The individual atoms getting polarized under the influence of the incident electric field make the planar structure a Huygen's surface [24].

A sharp dip in S_{21} is observed at 1.8 GHz. But this result is obtained upon normal wave incidence. In the case of our planar lens, being illuminated by the bow-tie antenna, the angle of incidence is not always perpendicular. In a recent study by Ginis et al. [25], it has been shown analytically that very thin metasurface can exhibit a broadband behaviour irrespective of the resonant nature of the unit cell. This is evident from our experimental results presented in Section 3.

The distance of the lens from the bow-tie antenna has been determined by simulation for minimum reflection from the lens surface and maximum gain over the bandwidth. The lens response to dominant polarization component of electric field is shown in Fig. 7. The horizontal axis represents distance along the antenna, and the vertical axis represents distance away from the antenna. The designed bow-tie antenna is placed along the horizontal axis. Figs. 7(c) and 7(d) show the bow-tie antenna with the lens placed along the x axis at 30 mm distance on the vertical axis. The phase of the E_x component of electric field vector emanating from the bow tie is shown. The bow-tie antenna has a spherical wavefront in the near field. The manipulation of the wavefront emerging out of the lens results in an increase in boresight directivity throughout the band.

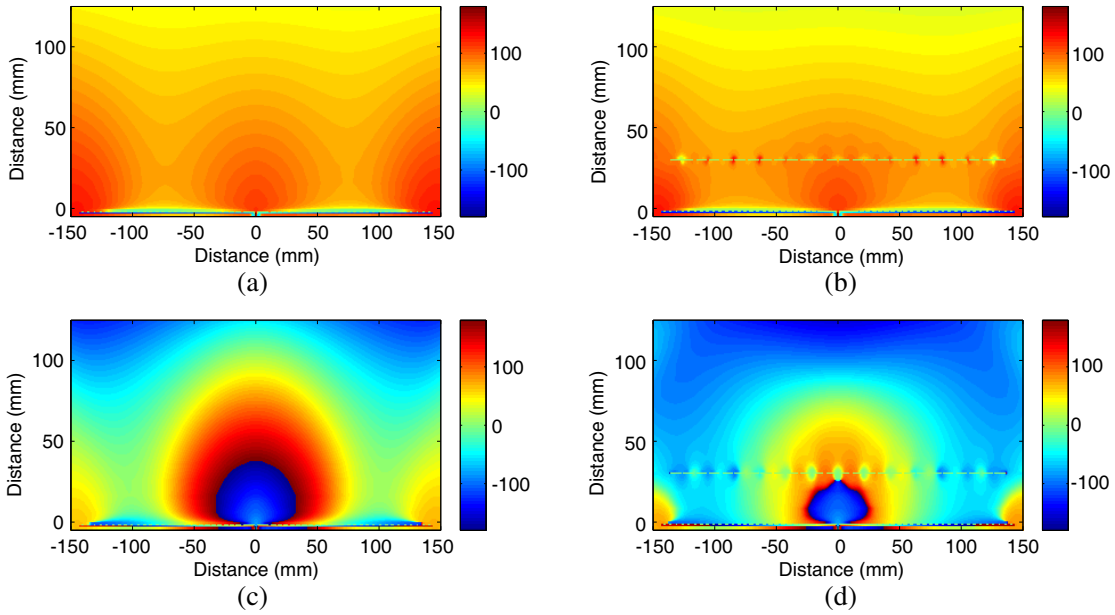

Figure 7. Phase manipulation by the lens at different frequencies. Phase of E_x at 500 MHz, in the near field of bow-tie antenna: (a) without lens, (b) with lens. Phase of E_x at 2 GHz, in the near field of bow-tie antenna: (c) without lens, (d) with lens.

3. EXPERIMENTAL RESULTS AND DISCUSSIONS

3.1. Return Loss and Input Impedance

The return loss for the concerned frequency range is shown in Fig. 8. The plot shows an ultra-wide impedance bandwidth extending from 300 MHz to 3 GHz. It is seen that the presence of the metamaterial has not affected the bandwidth. So the reflections from the lens' surface is negligible.

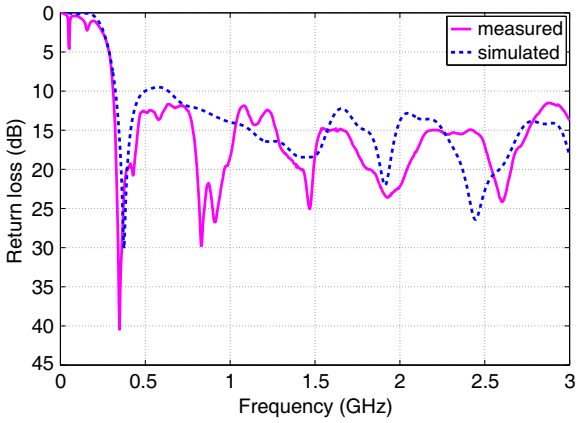

Figure 8. Return loss vs. frequency.

3.2. Realized Gain, Radiation Pattern and Front-to-Back Ratio

Figure 9 shows the antenna gain pattern in E- and H-planes for the entire frequencies of interest and compares it with the normal bow tie. Comparing H-plane pattern of the bow tie in Fig. 9(a) with that of lens antenna in Fig. 9(b) and E-plane pattern of the bow tie in Fig. 9(c) with that of lens antenna in

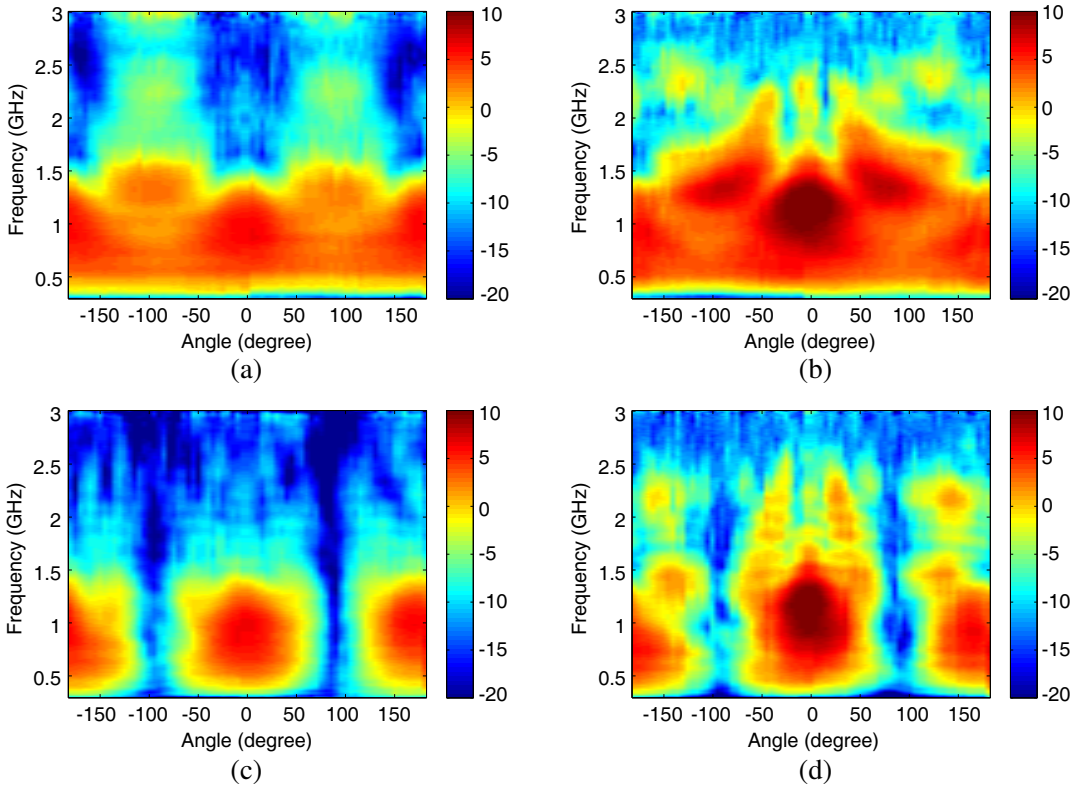

Figure 9. Measured radiation pattern in the UHF band. H-plane pattern of bow tie: (a) without lens and (b) with lens. E-plane pattern of bow tie: (c) without lens and (d) with lens.

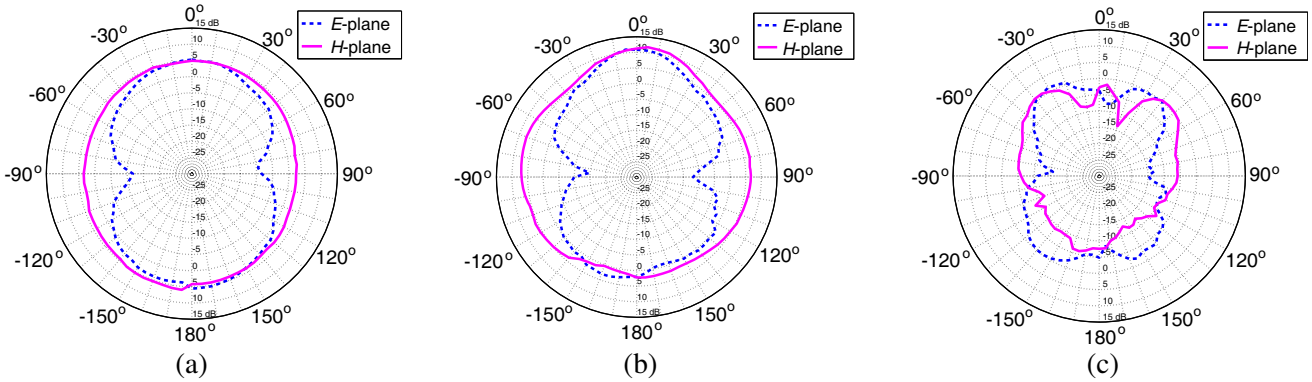

Figure 10. Radiation pattern in E and H plane at selected frequencies.

Fig. 9(d), the improvement in boresight gain is clearly appreciable. The measured peak gain is 11.52 dB at 1.124 GHz. The maximum gain obtained without lens is 6.45 dB at 914 MHz. Figure 9 shows a clear improvement in gain at 0 deg (boresight) at all frequencies, and the gain is improved by at least 5 dB at frequencies above 1.2 GHz as evident from Fig. 11(a).

Radiation patterns of the antenna at 500 MHz, 1.2 GHz, and 2 GHz are shown in Fig. 10. At 2 GHz, the antenna's major beam splits, and boresight gain gradually decreases at higher frequencies. Nevertheless, it is useful for applications as ground penetrating radar, because higher frequency signals do not penetrate much into the ground. So, decrease in gain at those frequencies is tolerable.

Front-to-back ratio is defined by the ratio of gain in the boresight direction to that in the back side of the antenna. The normal bow-tie antenna has a front-to-back ratio close to 0 dB as evident from the

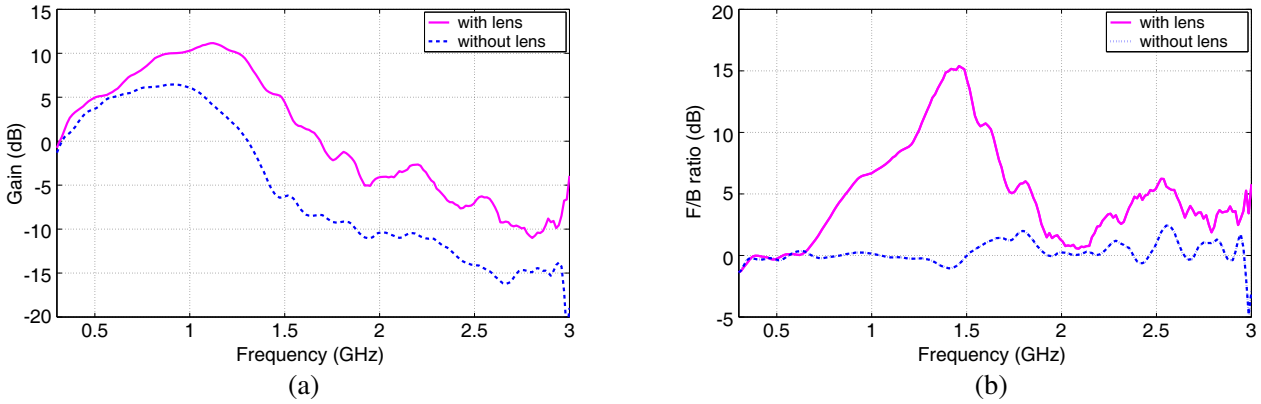

Figure 11. Comparison of measured gain and front-to-back ratio. (a) Measured realized gain. (b) Measured front-to-back ratio.

measurements. An improvement of up to 16 dB is obtained for the front-to-back ratio by using the lens as seen in Fig. 11(b).

3.3. Radiation Efficiency

Radiation efficiency measurement is carried out using the modified Wheeler cap method for UWB antennas outlined in [26] by Schantz. For this, a hollow metallic sphere of 50 cm diameter is used as shown in Fig. 12(a). The radius r of the metallic shell is chosen such that $r > \lambda/2\pi$ at the lowest frequency of operation. For the calculation of radiation efficiency, two sets of measurements are needed: one is reflection coefficient of the antenna in free space, and the other is reflection coefficient of the antenna inside the metallic shell centered at the origin.

If S_{11FS} is the measured reflection coefficient of the antenna in free space and S_{11WC} the measured reflection coefficient of the antenna inside the shell, then the radiation efficiency e_r is calculated using the formula [26]:

$$e_r = \sqrt{\left(1 - |S_{11FS}|^2\right)\left(|S_{11WC}|^2 - |S_{11FS}|^2\right)} \tag{3}$$

Figure 12(b) shows the radiation efficiency of the antenna. It can be seen that the efficiency of the designed bow-tie antenna with metamaterial lens is greater than 68.5% from 300 MHz to 2.2 GHz.

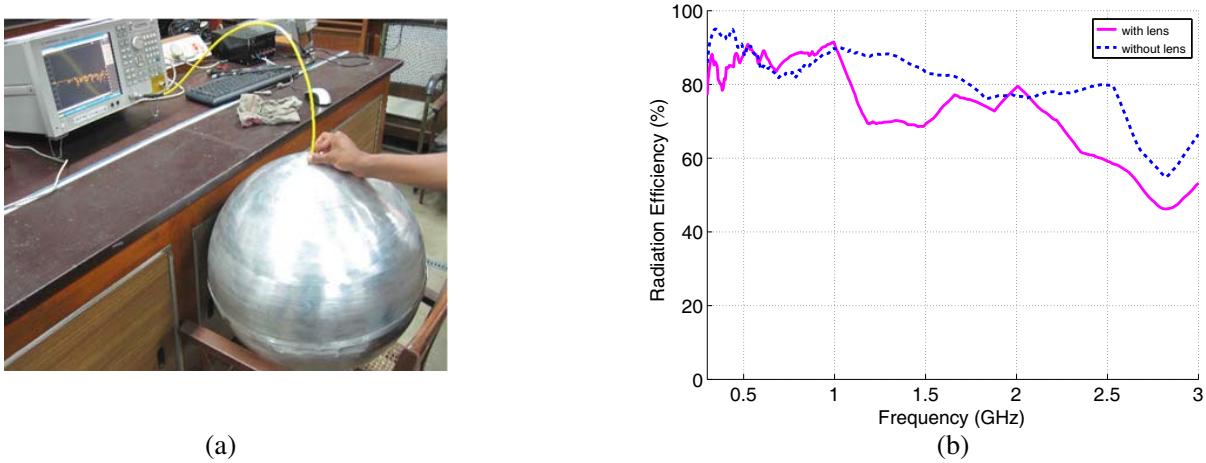

Figure 12. Radiation efficiency by using Schantz cap method for UWB antennas. (a) Radiation efficiency measurement setup. (b) Radiation efficiency vs frequency.

Efficiency drops to 46.2% at 2.8 GHz. Efficiency of the bow-tie antenna with lens is less than that without lens in most of the band because of the losses within the metamaterial.

3.4. GPR Experiment

An experimental GPR has been set up with the fabricated bow-tie antenna with lens and a hand-held vector network analyzer as shown in Fig. 13(a). This GPR is used to detect an object buried at a depth of 20 cm in a test bed filled with sand. Fig. 13(b) shows the measured GPR B-scan image of the object. The target is a metallic hollow rectangular object of size $42 \times 20 \times 11\,\text{cm}^3$ shown in the inset of the same figure. A brief description of this measurement is given below.

This is a stepped frequency continuous wave (SFCW) type radar. The whole setup, shown in the figure, is mobile, and the lowest rack contains the antenna with lens just touching the ground. The antenna is connected to port 1 of Vector Network Analyzer (Agilent FieldFox VNA-N9926A). The VNA is interfaced with the laptop on the top rack to acquire complex reflection coefficient data. The data are acquired on regular interval as we move the GPR over the linear track on the surface where the target is buried. Each measurement instance is called an A-scan. These frequency domain data are then inverse Fourier transformed to extract the depth information. The aggregation of all the A-scan, after applying some data processing algorithms, gives the image of the target. This is called the B-scan image and shown in Fig. 13(b).

3.5. Comparison

The designed antenna has a very compact size and very good gain compared to the other antennas found in literature. The size and features of this antenna are compared with the other antennas in the literature in Table 2. The work presented in this paper can cover the UHF bandwidth with the highest gain obtained in the band while the size of the antenna is only 0.3λ at the lowest frequency of operation.

Table 2. Comparison with other GPR antennas found in literature.

Ref.	Type	Lowest operating frequency	Highest operating frequency	Max. gain in the operating bandwidth	Front-to-back ratio	Size
[4]	RC loaded bowtie	500 MHz	5 GHz	Not known	Not known	50 cm
[27]	wire bowtie	500 MHz	5 GHz	Not known	Not known	50 cm
[3]	Resistive loaded bowtie	500 MHz	5 GHz	Not known	Not known	$23 \times 7\,\text{cm}^2$
[8]	Cavity-backed logarithmic spiral	400 MHz	3.8 GHz	6.6 dB	15 dB	$61 \times 29 \times 18\,\text{cm}^3$
[6]	Resistive loaded Vee dipole	500 MHz	8 GHz	5 dB	Not known	$17.15 \times 11.43\,\text{cm}^2$
[1]	Cavity backed Resistive loaded half-ellipse bowtie	250 MHz	750 MHz	Not known	Not known	$30 \times 18\,\text{cm}^2$
This work	bowtie without lens	300 MHz	3 GHz	6.45 dB	0 dB	$30 \times 23\,\text{cm}^2$
This work	bowtie with lens	300 MHz	3 GHz	11.52 dB	15.39 dB	$30 \times 23\,\text{cm}^2$

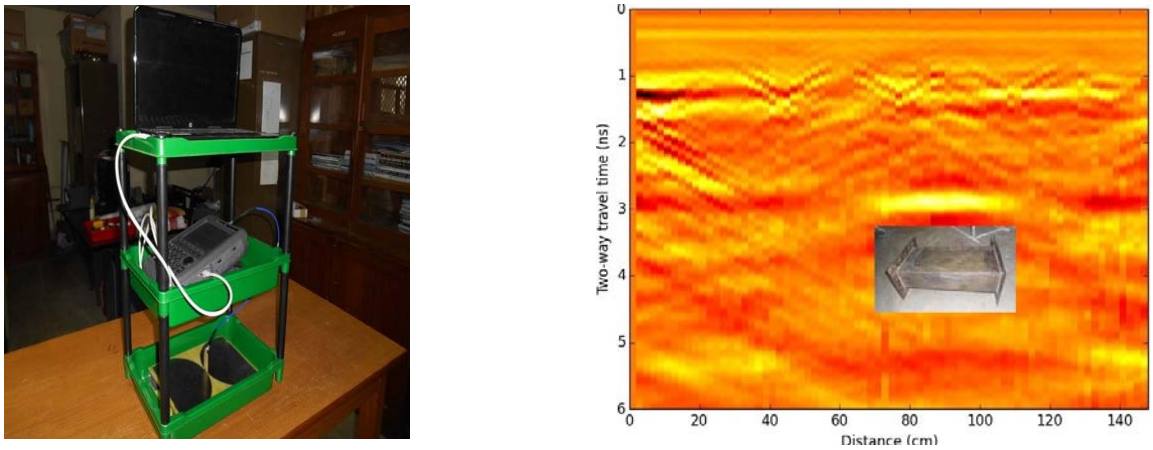

(a) (b)

Figure 13. GPR experiment. (a) Experimental GPR setup. (b) GPR B-scan image of a target buried in sand.

4. CONCLUSION

A compact printed lens antenna for UHF band has been presented. From the measurements it has been verified that by the use of a lens, both the gain and front-to-back ratio have been improved. An improvement in gain up to 5 dB is obtained compared to a bow-tie antenna without lens. The improvement in front-to-back ratio is up to 16 dB. Thus, omnidirectional radiation from a bow-tie antenna can be made directive by this technique. The antenna is also compact in size compared to other antennas found in the literature, considering its lowest frequency of operation. The antenna is suitable for UHF band, and its application in ground penetrating radar is demonstrated.

REFERENCES

1. Wu, B., Y. Ji, and G. Fang, "Analysis of GPR UWB half-ellipse antennas with different heights of backed cavity above ground," *IEEE Antennas and Wireless Propagation Letters*, Vol. 9, 130–133, 2010. [Online]. Available: http://ieeexplore.ieee.org/lpdocs/epic03/wrapper.htm?arnumber=5424004.
2. Wang, J., Y. Su, C. Huang, M. Lu, and Y. Li, "Design of bow-tie antenna with high radiating efficiency for impulse GPR," *2012 IEEE International Geoscience and Remote Sensing Symposium*, 594–597, Jul. 2012. [Online]. Available: http://ieeexplore.ieee.org/lpdocs/epic03/wrapper.htm?arnumber=6351524.
3. Lestari, A. A., E. Bharata, A. B. Suksmono, A. Kurniawan, A. G. Yarovoy, and L. P. Ligthart, "A modified bow-tie antenna for improved pulse radiation," *IEEE Transactions on Antennas and Propagation*, Vol. 58, No. 7, 2184–2192, Jul. 2010. [Online]. Available: http://ieeexplore.ieee.org/lpdocs/epic03/wrapper.htm?arnumber=5453013.
4. Lestari, A., A. Yarovoy, and L. Ligthart, "RC-loaded bow-tie antenna for improved pulse radiation," *IEEE Transactions on Antennas and Propagation*, Vol. 52, No. 10, 2555–2563, Oct. 2004. [Online]. Available: http://ieeexplore.ieee.org/lpdocs/epic03/wrapper.htm?arnumber=1341609.
5. Uduwawala, D., M. Norgren, P. Fuks, and A. Gunawardena, "A deep parametric study of resistor-loaded bow-tie antennas for ground-penetrating radar applications using FDTD," *IEEE Transactions on Geoscience and Remote Sensing*, Vol. 42, No. 4, 732–742, Apr. 2004. [Online]. Available: http://ieeexplore.ieee.org/lpdocs/epic03/wrapper.htm?arnumber=1288368.
6. Kim, K. and W. Scott, "Design of a resistively loaded Vee dipole for ultrawide-band ground-penetrating radar applications," *IEEE Transactions on Antennas and Propagation*, Vol. 53, No. 8,

2525–2532, Aug. 2005. [Online]. Available: http://ieeexplore.ieee.org/lpdocs/epic03/wrapper.htm?arnumber=1492596.

7. Yang, H. and K. Kim, "Ultra-wideband impedance matching technique for resistively loaded Vee dipole antenna," *IEEE Transactions on Antennas and Propagation*, Vol. 61, No. 11, 5788–5792, Nov. 2013. [Online]. Available: http://ieeexplore.ieee.org/lpdocs/epic03/wrapper.htm?arnumber=6573326.
8. Thaysen, J., "A logarithmic spiral antenna for 0.4 to 3.8 GHz," *Applied Microwave and Wireless*, Vol. 13, No. 2, 32–45, 2001.
9. Kock, W., "Metal-lens antennas," *Proceedings of the IRE*, Vol. 34, No. 11, 828–836, Nov. 1946. [Online]. Available: http://ieeexplore.ieee.org/lpdocs/epic03/wrapper.htm?arnumber=1696976.
10. Pozar, D., "Flat lens antenna concept using aperture coupled microstrip patches," *Electronics Letters*, Vol. 32, No. 23, 2109, 1996. [Online]. Available: http://digital-library.theiet.org/content/journals/10.1049/el19961451.
11. Alù, A., M. G. Silveirinha, A. Salandrino, and N. Engheta, "Epsilon-near-zero metamaterials and electromagnetic sources: Tailoring the radiation phase pattern," *Physical Review B*, Vol. 75, No. 15, 155410, Apr. 2007. [Online]. Available: http://link.aps.org/doi/10.1103/PhysRevB.75.155410.
12. Zhu, H. L., S. W. Cheung, K. L. Chung, and T. I. Yuk, "Linear-to-circular polarization conversion using metasurface," *IEEE Transactions on Antennas and Propagation*, Vol. 61, No. 9, 4615–4623, Sep. 2013. [Online]. Available: http://ieeexplore.ieee.org/lpdocs/epic03/wrapper.htm?arnumber=6529103.
13. Zhou, B. and T. J. Cui, "Directivity enhancement to vivaldi antennas using compactly anisotropic zero-index metamaterials," *IEEE Antennas and Wireless Propagation Letters*, Vol. 10, 326–329, 2011. [Online]. Available: http://ieeexplore.ieee.org/lpdocs/epic03/wrapper.htm?arnumber=5749686.
14. Qi, M. Q., W. X. Tang, H.-X. Xu, H. F. Ma, and T. J. Cui, "Tailoring radiation patterns in broadband with controllable aperture field using metamaterials," *IEEE Transactions on Antennas and Propagation*, Vol. 61, No. 11, 5792–5798, Nov. 2013. [Online]. Available: http://ieeexplore.ieee.org/lpdocs/epic03/wrapper.htm?arnumber=6576199.
15. Vallecchi, A., J. R. de Luis, F. Capolino, and F. de Flaviis, "Low profile fully planar folded dipole antenna on a high impedance surface," *IEEE Transactions on Antennas and Propagation*, Vol. 60, No. 1, 51–62, Jan. 2012. [Online]. Available: http://ieeexplore.ieee.org/lpdocs/epic03/wrapper.htm?arnumber=6018997.
16. Erentok, A., R. W. Ziolkowski, J. A. Nielsen, R. B. Greegor, C. G. Parazzoli, M. H. Tanielian, S. A. Cummer, B.-I. Popa, T. Hand, D. C. Vier, and S. Schultz, "Lumped element-based, highly sub-wavelength, negative index metamaterials at UHF frequencies," *Journal of Applied Physics*, Vol. 104, No. 3, 034901, 2008. [Online]. Available: http://scitation.aip.org/content/aip/journal/jap/104/3/10.1063/1.2959377.
17. Erentok, A. and R. W. Ziolkowski, "Metamaterial-inspired efficient electrically small antennas," *IEEE Transactions on Antennas and Propagation*, Vol. 56, No. 3, 691–707, Mar. 2008. [Online]. Available: http://ieeexplore.ieee.org/lpdocs/epic03/wrapper.htm?arnumber=4463892.
18. Ajith, K. K. and A. Bhattacharya, "Improved ultra-wide bandwidth bow-tie antenna with metamaterial lens for GPR applications," *Proceedings of the 15th International Conference on Ground Penetrating Radar*, 739–744, Jun. 2014. [Online]. Available: http://ieeexplore.ieee.org/lpdocs/epic03/wrapper.htm?arnumber=6970525.
19. DuHamel, R. and D. Isbell, "Broadband logarithmically periodic antenna structures," *IRE International Convention Record*, Vol. 5, 119–128, Institute of Electrical and Electronics Engineers, 1958. [Online]. Available: http://ieeexplore.ieee.org/lpdocs/epic03/wrapper.htm?arnumber=1150566.
20. Carrel, R., "The characteristic impedance of two infinite cones of arbitrary cross section," *IRE Transactions on Antennas and Propagation*, Vol. 6, No. 2, 197–201, Apr. 1958. [Online]. Available: http://ieeexplore.ieee.org/lpdocs/epic03/wrapper.htm?arnumber=1144578.
21. Chen, E. and S. Chou, "Characteristics of coplanar transmission lines on multilayer substrates: Modeling and experiments," *IEEE Transactions on Microwave Theory and Techniques*, Vol. 45,

No. 6, 939–945, Jun. 1997. [Online]. Available: http://ieeexplore.ieee.org/lpdocs/epic03/wrapper.htm?arnumber=588606.

22. Gevorgian, S. and H. Berg, "Line capacitance and impedance of coplanar-strip waveguides on substrates with multiple dielectric layers," *31st European Microwave Conference, 2001*, 1–4, Oct. 2001. [Online]. Available: http://ieeexplore.ieee.org/lpdocs/epic03/wrapper.htm?arnumber=4140229.
23. Simons, R. N., *Coplanar Waveguide Circuits, Components, and Systems*, ser. Wiley Series in Microwave and Optical Engineering, John Wiley & Sons, Inc., New York, USA, Mar. 2001. [Online]. Available: http://doi.wiley.com/10.1002/0471224758.
24. Pfeiffer, C. and A. Grbic, "Metamaterial huygens surfaces: Tailoring wave fronts with reflectionless sheets," *Physical Review Letters*, Vol. 110, No. 19, 197401, May 2013. [Online]. Available: http://link.aps.org/doi/10.1103/PhysRevLett.110.197401.
25. Ginis, V., P. Tassin, T. Koschny, and C. M. Soukoulis, "Broadband metasurfaces enabling arbitrarily large delay-bandwidth products," *Applied Physics Letters*, Vol. 108, No. 3, 031601, Jan. 2016. [Online]. Available: http://scitation.aip.org/content/aip/journal/apl/108/3/10.1063/1.4939979.
26. Schantz, H., "Radiation efficiency of UWB antennas," *2002 IEEE Conference on Ultra Wideband Systems and Technologies (IEEE Cat. No. 02EX580)*, 351–355, 2002. [Online]. Available: http://ieeexplore.ieee.org/lpdocs/epic03/wrapper.htm?arnumber=1006392.
27. Lestari, A., A. Yarovoy, and L. Ligthart, "Adaptive wire bow-tie antenna for GPR applications," *IEEE Transactions on Antennas and Propagation*, Vol. 53, No. 5, 1745–1754, May 2005. [Online]. Available: http://ieeexplore.ieee.org/lpdocs/epic03/wrapper.htm?arnumber=1427933.